Comparative study on characteristics of Si-based AlGaN/GaN recessed MIS-HEMTs with HfO_2 and Al_2O_3 gate insulators*

Yao-Peng Zhao(赵垚澎), Chong Wang(王冲)†, Xue-Feng Zheng(郑雪峰)‡, Xiao-Hua Ma(马晓华), Kai Liu(刘凯), Ang Li(李昂), Yun-Long He(何云龙), and Yue Hao(郝跃)

Key Laboratory of Wide Band-Gap Semiconductor Materials and Devices, School of Microelectronics, Xidian University, Xi'an 710071, *China*

(Received 18 March 2020; revised manuscript received 24 April 2020; accepted manuscript online 28 April 2020)

Two types of enhancement-mode (E-mode) AlGaN/GaN metal–insulator–semiconductor high-electron-mobility transistors (MIS-HEMTs) with different gate insulators are fabricated on Si substrates. The HfO_2 gate insulator and the Al_2O_3 gate insulator each with a thickness of 30 nm are grown by the plasma-enhanced atomic layer deposition (PEALD). The energy band diagrams of two types of dielectric MIS-HEMTs are compared. The breakdown voltage (V_{BR}) of HfO_2 dielectric layer and Al_2O_3 dielectric layer are 9.4 V and 15.9 V, respectively. With the same barrier thickness, the transconductance of MIS-HEMT with HfO_2 is larger. The threshold voltage (V_{th}) of the HfO_2 and Al_2O_3 MIS-HEMT are 2.0 V and 2.4 V, respectively, when the barrier layer thickness is 0 nm. The *C–V* characteristics are in good agreement with the V_{th}'s transfer characteristics. As the barrier layer becomes thinner, the drain current density decreases sharply. Due to the dielectric/AlGaN interface is very close to the channel, the scattering of interface states will lead the electron mobility to decrease. The current collapse and the R_{on} of Al_2O_3 MIS-HEMT are smaller at the maximum gate voltage. As Al_2O_3 has excellent thermal stability and chemical stability, the interface state density of Al_2O_3/AlGaN is less than that of HfO_2/AlGaN.

Keywords: AlGaN/GaN, enhancement-mode, MIS-HEMT, HfO_2, Al_2O_3

PACS: 73.40.Kp, 73.40.Rw, 73.40.Qv, 73.61.Ey **DOI:** 10.1088/1674-1056/ab8daa

1. Introduction

GaN-based high electron mobility transistors (HEMTs) are well suitable for the applications in power switching devices.[1–4] Enhancement-mode (E-mode) HEMT is very important for the switch power supply which can reduce power loss by keeping the device closed at zero gate bias.[5–7] The gate-recessed metal–insulator–semiconductor (MIS) structure is considered as an important structure to realize the E-mode AlGaN/GaN power devices because of the high threshold voltage (V_{th}) and the high drain current density.[8]

Gate dielectric material is of vital importance for MIS-HEMTs.[9,10] The HfO_2 has a relatively high dielectric constant of 22 and lower band gap of 6.0 eV as a new-type high-*k* material.[11] The Al_2O_3 has a relatively low dielectric constant of 9.3 and larger band gap of 8.8 eV as a frequently used gate dielectric. Difference in gate dielectric has a great influence on the characteristics of devices. The dielectric constant corresponds to the gate capacitance, and the gate can control the two-dimensional electron gas (2DEG) in the channel more easily when the gate dielectric constant is higher.[12] The band gap corresponds to the positive gate voltage capability of the gate dielectric. A larger band gap means a higher positive gate voltage capability.[13] Choi, *et al.* have reported the E-mode MIS-HEMT with dual gate dielectric of SiN_x and HfO_2.[14] However, few articles have reported the comparison of characteristics between the HfO_2 and the Al_2O_3 gate dielectric for the gate recessed MIS-HEMT.

In this paper, two types of HEMTs are designed and fabricated, known as gate-recessed MIS-HEMTs with HfO_2 and Al_2O_3 gate dielectric grown by plasma-enhanced atomic layer deposition (PEALD). There are three etching depths in the two types of MIS-HEMTs. The energy band diagrams of the two types of MIS-HEMTs are compared with each other. Moreover, the direct current (DC) characteristics and pulse characteristics are compared and analyzed.

2. Device fabrication

The AlGaN/GaN heterojunction structure used in this paper was grown on a silicon (111) substrate by the metal organic chemical vapor deposition (MOCVD) method. The wafer consisted of an AlN nucleation layer, an AlGaN gradient layer in which the Al percentage ranges from 8% to 0, a 2-µm-thick C-doped GaN layer, a 160-nm-thick undoped GaN channel, and a 25-nm-thick undoped AlGaN barrier layer. Room temperature hall measurements of the epi-wafer yielded an electron sheet density of 9.0×10^{12} cm^{-2} and an electron mobility of 2000 cm^2/V·s.

The mesa area was formed by using BCl_3/Cl_2 plasma etching in an inductively coupled plasma (ICP) system followed by the drain/source ohmic contact formation by us-

*Project supported by the National Natural Science Foundation of China (Grant Nos. 61974111, 11690042, and 61974115), the National Pre-research Foundation of China (Grant No. 31512050402), and the Fund of Innovation Center of Radiation Application, China (Grant No. KFZC2018040202).

†Corresponding author. E-mail: chongw@xidian.edu.cn

‡Corresponding author. E-mail: xfzheng@mail.xidian.edu.cn

© 2020 Chinese Physical Society and IOP Publishing Ltd

ing Ti/Al/Ni/Au (30 nm/180 nm/40 nm/ 60 nm) annealed at 840 ℃ for 30 s. A 60-nm-thick Si_3N_4 layer was deposited on a surface by the plasma-enhanced chemical vapor deposition (PECVD), and the Si_3N_4 of the gate area was removed by CF_4 plasma etching. The gate-recessed MIS-HEMT was etched by using BCl_3 and Cl_2. The barrier layer thickness values were 6 nm, 3 nm, and 0 nm, respectively. The next step was high temperature (300 ℃) N_2 plasma treatment in the recessed-gate region by using the plasma enhanced atomic layer deposition (PEALD) with the treatment power of 150 W for 10 min. Then, the HfO_2 and Al_2O_3 dielectric layer were deposited separately to a thickness of 30 nm. Then, Ni/Au E-beam evaporation and lift off were carried out to form the gate electrode. Finally, post gate annealing (PGA) treatment of 400 ℃ in ambient N_2 for 5 min was implemented for reducing the interface state density.[15] The L_g, L_{gd}, and L_{ds} of the devices were 1.0 μm, 3.5 μm, and 7.0 μm, respectively. The W_g of the device was 50 μm. Figure 1 shows the schematic cross-sectional structure of the gate-recessed MIS-HEMT. Figure 2 shows the photomicrograph of the MIS-HEMT and the focused ion beam (FIB) cross-sectional view of the device's gate corner of the gate-recessed MIS-HEMT of HfO_2. The parameters of the devices were measured by Keithley 4200.

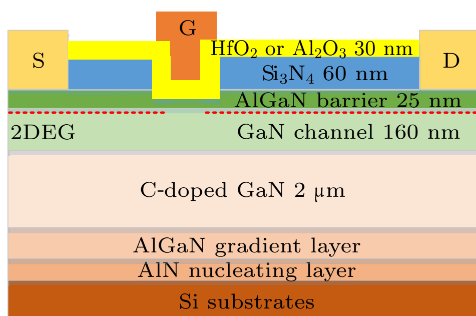

Fig. 1. Schematic cross-sectional structure of AlGaN/GaN gate-recessed MIS-HEMT.

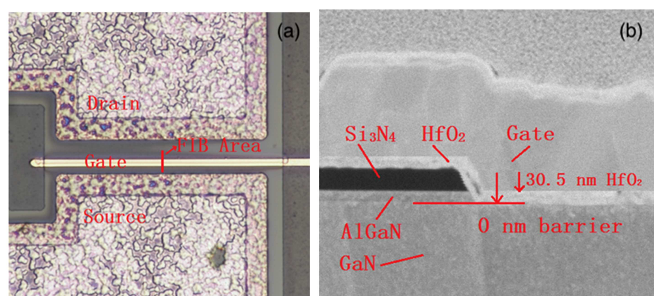

Fig. 2. Photomicrograph of (a) MIS-HEMT device and (b) FIB cross-sectional view of gate area.

3. Results and discussion

Due to the fact that the band gap of HfO_2 and Al_2O_3 are different, the energy band diagrams of the two types of MIS-HEMTs are different as shown in Fig. 3. The band gap of Al_2O_3 is 8.8 eV, much larger than 6.0 eV of HfO_2. However, the barrier height (ϕ_B) of Ni/Al_2O_3 is 3.5 eV, and the barrier height of Ni/HfO_2 is 3.25 eV for the Ni/Au gate.[16] The ΔE_{C1} is the conduction-band discontinuity between dielectric and AlGaN. The ΔE_{C1} of the $Al_2O_3/Al_{0.25}Ga_{0.75}N$ is 1.8 eV while the ΔE_{C1} of the $HfO_2/Al_{0.25}Ga_{0.75}N$ is 0.8 eV. Figure 3 shows that the barrier heights of the gate metals have almost the same depletion effect on the electrons in the channel. The capacitance of the dielectric mainly affects the electrons under the same gate voltage. The specific capacitance is shown in Fig. 6.

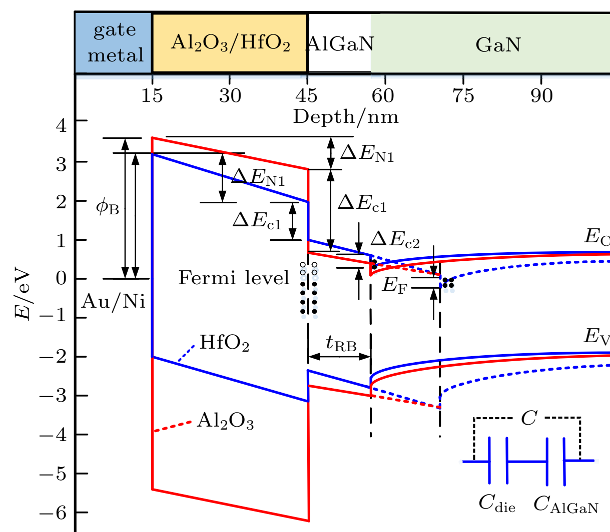

Fig. 3. Energy band diagram of AlGaN/GaN gate-recessed MIS-HEMT.

Figure 4 shows the molecular structure diagram of HfO_2/AlGaN and Al_2O_3/AlGaN interfaces. As the Hf atom is much larger than the Ga atom and N atom, there will be many hanging bonds on the N atoms at the HfO_2/AlGaN interface. On the other hand, the Al atoms are small and there are Al atoms in the AlGaN layer, so there are few hanging bonds on the N atoms at the HfO_2/AlGaN interface. The interface state density of the Al_2O_3/AlGaN is smaller than that of the HfO_2/AlGaN interface. This can be confirmed by the test results of current collapse in Fig. 9.

Figure 5 shows the curves of breakdown voltage (V_{BR}) between gate and source of the two types of MIS-HEMTs. Each structure of the three devices is tested. The average V_{BR} of HfO_2 dielectric layer and Al_2O_3 dielectric layer are 9.4 V and 15.9 V, respectively. As the band gap of HfO_2 and Al_2O_3 are 6.0 eV and 8.8 eV, respectively, the Al_2O_3 can withstand a larger gate voltage range. The gate voltage range of Al_2O_3 is closer to that of Si MOS device. The gate leakage of Al_2O_3 is smaller than that of HfO_2. As Al_2O_3 has a higher energy-band offset on the AlGaN layer, holes are more difficult to cross the barrier of Al_2O_3 and a low gate leakage current can be formed by weakening Fowler–Nordheim (FN) tunneling.[17] On the other hand, the Al_2O_3/AlGaN interface is better than the HfO_2/AlGaN interface as shown in Fig. 4.

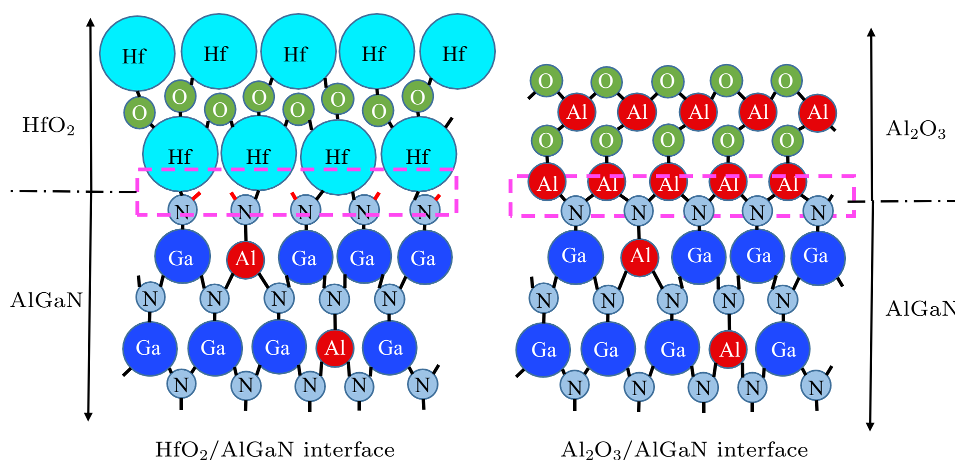

Fig. 4. Molecular structure diagram of HfO_2/AlGaN and Al_2O_3/AlGaN interfaces.

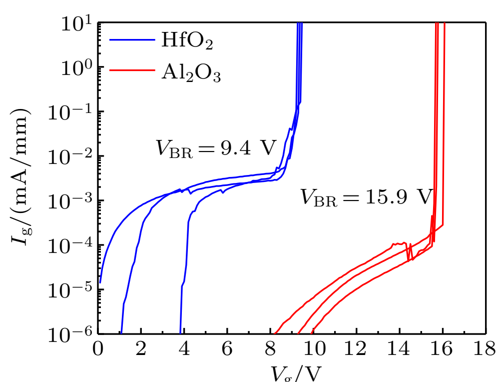

Fig. 5. Curves of dielectric layer breakdown voltage of devices.

For the MIS-HEMT with HfO_2, The drain current density and transconductance increase greatly after post-gate-annealing (PGA, 400 ℃, 5 min) treatment.[15] The threshold voltage (V_{th}) of the MIS-HEMT decreases after the PGA treatment. Figure 6 shows the comparisons of transfer characteristics between the HfO_2 and Al_2O_3 MIS-HEMTs with different etching depths after the PGA treatment. To protect the devices, the maximum gate voltage for the HfO_2 and Al_2O_3 MIS-HEMT are set to be +8 V and +15 V, respectively. Figure 6(a) shows that the drain current density of the HfO_2 and Al_2O_3 MIS-HEMT of 6-nm barrier thickness are 898 mA/mm and 905 mA/mm, respectively. Their V_{th} values are 0.1 V and 1.1 V, respectively. The peak transconductance of the HfO_2 MIS-HEMT is 189 mS/mm, which is much larger than 102 mS/mm of the Al_2O_3 MIS-HEMT. Because the dielectric constant of HfO_2 is 22, which is much larger than 9.3 of Al_2O_3, the dielectric capacitance and the transconductance of HfO_2 are also much larger than those of the Al_2O_3 MIS-HEMT. For an E-mode device, a smaller gate capacitance requires a higher voltage to yield the same amount of electrons under the gate, so the V_{th} of Al_2O_3 MIS-HEMT is larger.[18] Figures 6(b) and 6(c) show that the drain current density of the HfO_2 MIS-HEMT decreases to 610 mA/mm and 379 mA/mm for the barrier thickness of 3-nm and 0-nm barrier thickness, respectively. The current of Al_2O_3 MIS-HEMT also has a similar decreasing trend. The decrease of current is mainly due to the concentration and mobility of the 2DEG decreasing. When the barrier layer is thinner, the dielectric/AlGaN interface is very close to the channel, so the scattering of interface states will lead to the electron mobility to decrease.[19] The V_{th} of the HfO_2 and Al_2O_3 MIS-HEMT are 2.0 V and 2.4 V, respectively when the barrier thickness is 0 nm. In this case there is no 2DEG (two-dimensional electron gas) in the channel and the structure of the device is similar to the MOS structure. As the gate voltage increases, the gate capacitance can attract the electrons in GaN to connect the channel, but the concentration and mobility of electrons are not so high as those of 2DEG. Therefore, the characteristics of the device greatly decrease. Figure 6(d) shows that the V_{th} of the Al_2O_3 MIS-HEMT is larger and the transconductance of HfO_2 MIS-HEMT is larger when the barrier layer thickness is the same.

The *C–V* characteristics are shown in Fig. 7. The onset voltage (V_o) values of HfO_2 MIS-HEMTs are 0.2 V, 1.4 V, 1.9 V respectively corresponding to the different barrier thicknesses, which is in good agreement with the V_{th}'s transfer characteristic. Similarly, the V_o values of Al_2O_3 MIS-HEMTs are 0.8 V, 2.5 V, 3.0 V, respectively. A second slop exists when the barrier thickness is 6 nm.[20] The electrons in the channel reach the dielectric/AlGaN interface when the gate voltage increases, so the gate capacitance increases due to the series connection of the dielectric layer capacitance and barrier layer capacitance to the only dielectric layer capacitance.[15] For the MIS-HEMT with 3-nm and 0-nm barriers, the second slope is observed in none of the *C–V* curves. As the barrier layer is too thin, the electrons reach the dielectric/AlGaN interface directly. With the gate voltage increasing, the capacitance finally approaches to the dielectric layer capacitance which is 791 nF/cm^{-2} and 308 nF/cm^{-2} for the HfO_2 and Al_2O_3 MIS-HEMT, respectively. The dielectric constant of HfO_2 is 22 also much larger than 9.3 of Al_2O_3. There is also a good correspondence between gate capacitance and dielectric constant.

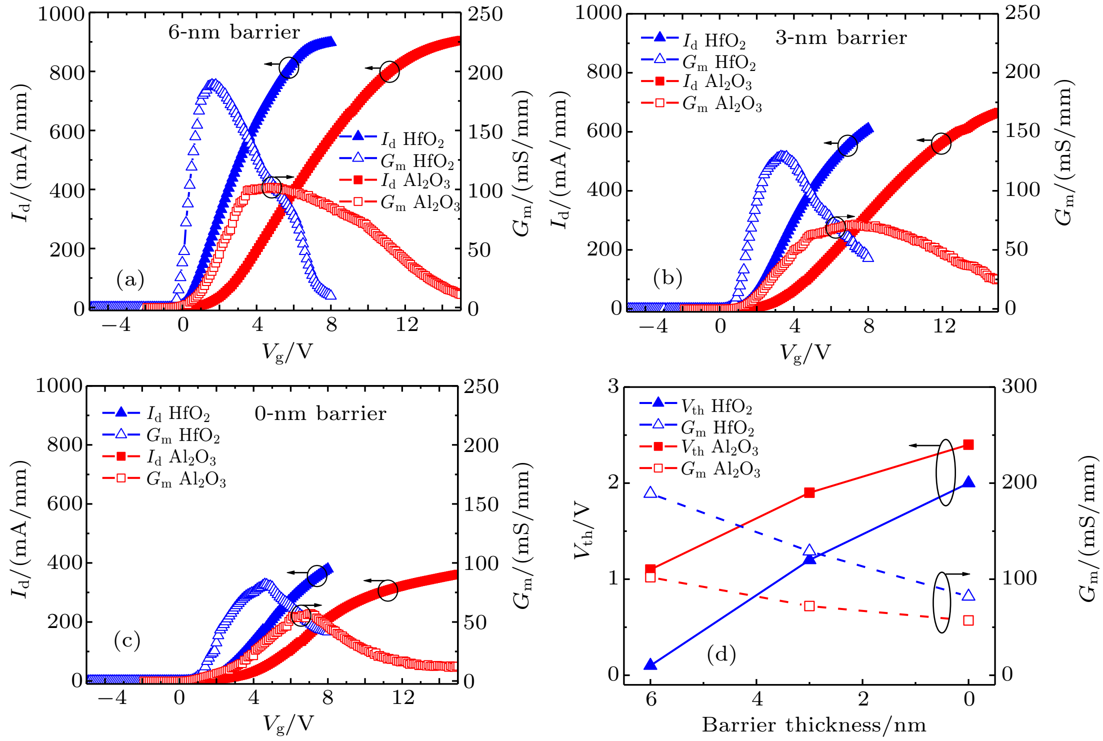

Fig. 6. Curves of transfer characteristics of recessed MIS-HEMT with (a) 6-nm-thick barrier, (b) 3-nm-thick barrier, and (c) 0-nm-thick barrier, and (d) change trend comparison chart of $V_{\rm th}$ and $G_{\rm m}$.

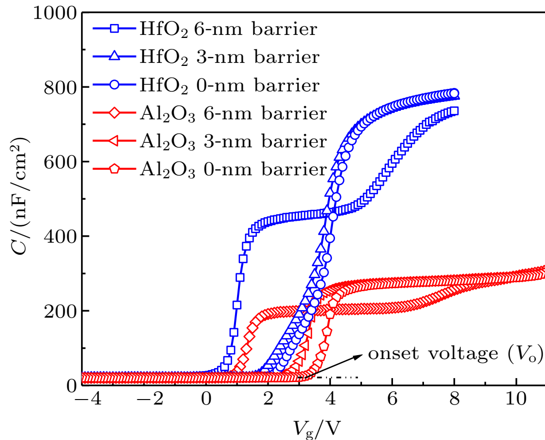

Fig. 7. The C–V curves of gate-recessed MIS-HEMT.

In order to change the mobility values of the devices, the FAT-FETs are tested by measuring I–V and C–V characteristics. The gate width ($W_{\rm G}$) is 100 μm, the gate length ($L_{\rm G}$) is 50 μm, and the $V_{\rm d}$ is 0.1 V.[21] As the device is biased in the linear range, the channel drift mobility can be expressed by

$$\mu = \frac{G_{\rm ch}L_{\rm G}}{W_{\rm G}CV_{\rm D}}. \quad (1)$$

According to Eq. (1), C is obtained from the C–V test results, and $G_{\rm ch}$ from the I–V test. The mobility curves are shown in Fig. 8. The peak mobility values of MIS-HEMT with a 6-nm-thick barrier layer are, respectively, 1134 cm^2/V·s of HfO_2 and 1129 cm^2/V·s of Al_2O_3. The mobility of MIS-HEMT with a 3-nm-thick barrier decreases to 876 cm^2/V·s, and sharply decrease to 118 cm^2/V·s when the barrier thickness is 0 nm. The scattering of electrons increases and the electron mobility is very low when there is a small quantity of 2DEG in the channel under the gate. The change rules of the electron mobility of the two types of MIS-HEMTs are basically the same.

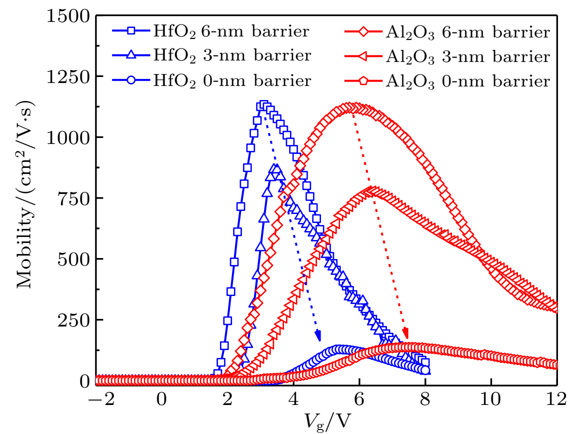

Fig. 8. Plots of drift mobility *versus* gate voltage $V_{\rm g}$ of electron for HfO_2 and Al_2O_3 barriers with different thickness values.

A dual-pulse current collapse test is performed on each of the devices, and the results are shown in Fig. 9. In the test, the pulse width is 5×10^{-7} s, with 1-ms period and the rise time and the decline time are both 1.5×10^{-7} s. In the current collapse test, selected are two static operating points, *i.e.*, the $(V_{\rm gs}, V_{\rm ds}) = (0,0)$ state and the $(V_{\rm gs}, V_{\rm ds}) = (-8,10)$ state. According to the measurement, the current collapses of 6-nm barrier MIS-HEMT are 7.3% and 6.7% for the HfO_2 and Al_2O_3, respectively. Their current collapses increase to 29.7% and 20.8% when the barrier layer is 0 nm. The current collapse of

HfO_2 MIS-HEMT is larger than that of Al_2O_3 MIS-HEMT, for there are more interface states at the HfO_2/AlGaN interface. When the barrier thickness is 0 nm, the trap state of HfO_2/GaN interface directly affects the electrons in the channel. The process of trap charge and discharge greatly influence the output current, so the collapse of HfO_2 MIS-HEMT reaches 29.7%. In addition, the specific on-resistance (R_{on}) can be obtained through the pulse output curve at (0, 0) state. The R_{on} values of the HfO_2 MIS-HEMT are 4.3 Ω·mm, 6.5 Ω·mm, and 9.2 Ω·mm, respectively, which are larger than those of Al_2O_3 MIS-HEMT. At the maximum gate voltage, the mobility of HfO_2 MIS-HEMT is lower than that of Al_2O_3 MIS-HEMT, so the R_{on} of HfO_2 MIS-HEMT is larger. Figure 10 shows the comparisons of change trend among the devices. At the same barrier layer thickness, the current collapses of Al_2O_3 MIS-HEMT are smaller mainly due to the better interface of Al_2O_3/AlGaN as Al_2O_3 has excellent thermal stability (amorphous up to at least 1000 ℃) and chemical stability.[16] Also the Al element is contained in Al_2O_3 and there are many hanging bonds on the N atoms at the HfO_2/AlGaN interface, so the interface states of Al_2O_3/AlGaN are less than those of HfO_2/AlGaN. The interface states are in the form of trap states and fixed charges. The interface state density can be reduced effectively by filling the nitrogen vacancies through oxygen atoms into the HfO_2 and Al_2O_3 layer and reducing oxygen-related defects at the dielectric/AlGaN interface.[15] It can be concluded that the interface states under the gate greatly influence the current collapse.

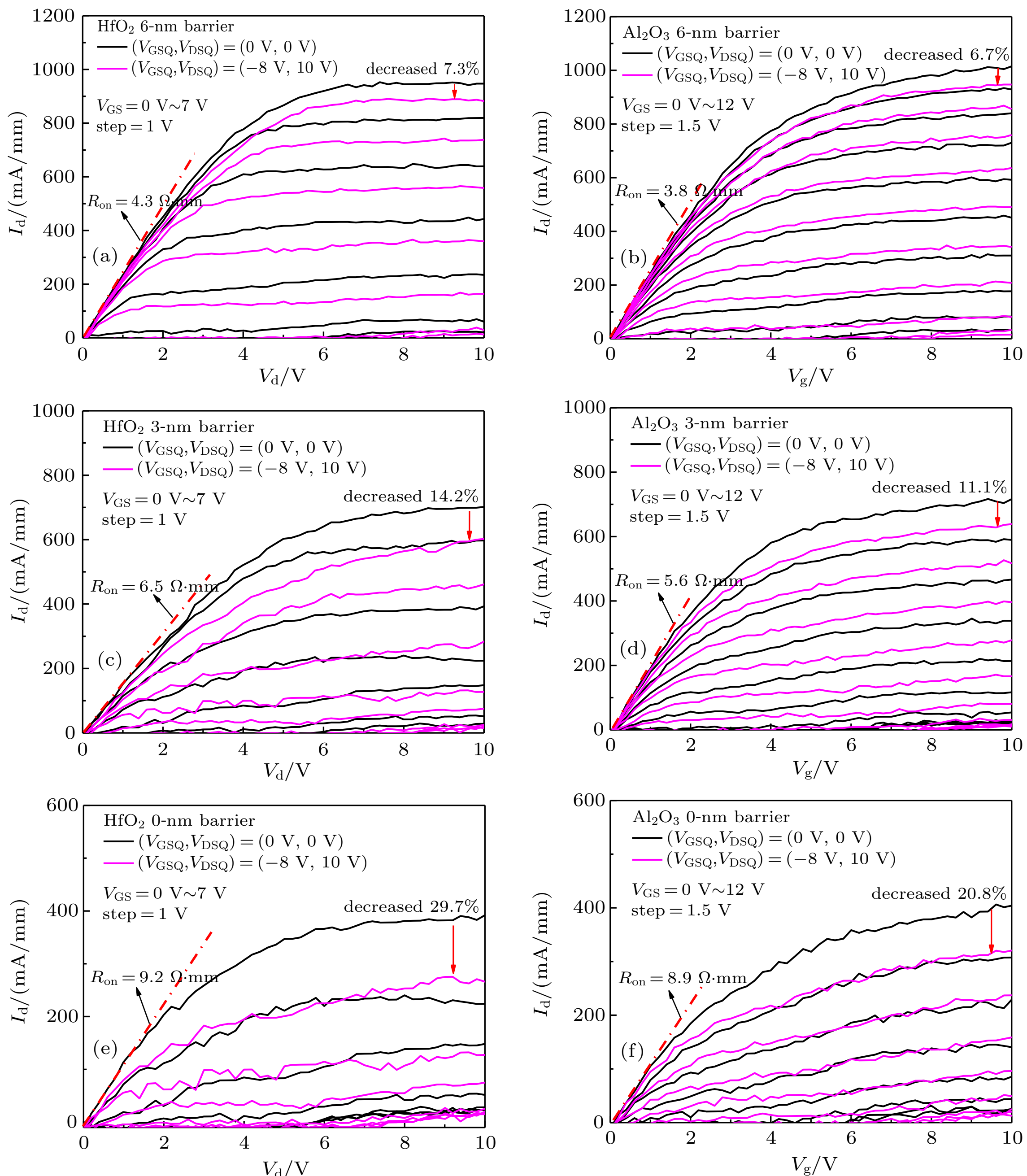

Fig. 9. Pulsed output current curves of devices.

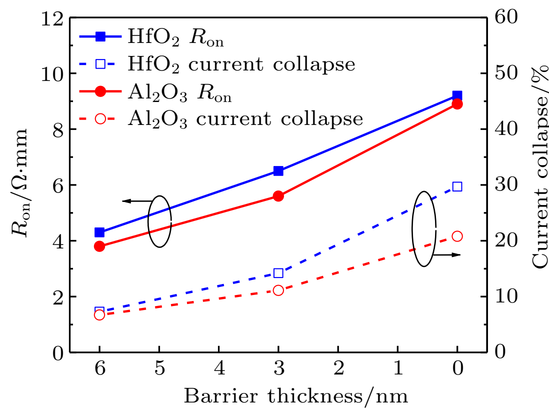

Fig. 10. Comparisons of change trend of R_{on} and current collapse betwen HfO_2 and Al_2O_3 MIS-HEMTs at maximum gate voltage.

4. Conclusions

The AlGaN/GaN MIS-HEMTs with three different etching depths by using HfO_2 and Al_2O_3 gate insulators are fabricated on Si substrates. The barrier layer thickness values are 6 nm, 3 nm, and 0 nm respectively. The energy band diagrams of two types of dielectric MIS-HEMTs are compared. The V_{BR} of the HfO_2 and Al_2O_3 gate are 9.4 V and 15.9 V, respectively. At the same barrier thickness, the transconductance of MIS-HEMT with HfO_2 is larger. The V_{th} of the HfO_2 and Al_2O_3 MIS-HEMTs are 2.0 V and 2.4 V, respectively, when the barrier thickness is 0 nm. The C–V characteristics are in good agreement with the V_{th}'s transfer characteristics. When the barrier layer is thinner, the drain current density decreases sharply. The current collapse and R_{on} of Al_2O_3 MIS-HEMT are smaller at the maximum gate voltage. The interface states of Al_2O_3/AlGaN are less than those of HfO_2/AlGaN, for the Al_2O_3 has excellent thermal stability and chemical stability and the Al_2O_3 and AlGaN both contain the Al element.

References

[1] Hua M Y, Wei J, Bao Q L, Zhang Z F, Zheng Z Y and Chen Kevin J 2018 *IEEE T. Electron. Dev.* **39** 413

[2] Nifa I, Leroux C, Torres A, Charles M, Reimbold G, Ghibaudo G and Bano E 2019 *Microelectron. Eng.* **215** 110976

[3] Fei X X, Wang Y, Luo X, Cao F and Yu C H 2018 *Superlattice Microst.* **114** 314

[4] Garcia F, Shamsir S and Islam S K 2019 *Solid-State Electron.* **151** 52

[5] Shi Y J, Huang S, Bao Q L, Wang X H, Wei K, Jiang H J, Li J F, Zhao C, Li S M, Zhou Y, Gao H W, Sun Q, Yang H, Zhang J H, Chen W J, Zhou Q, Zhang B and Liu X Y 2016 *IEEE T. Electron. Dev.* **63** 614

[6] Wang H Y, Wang J Y, Li M J, Cao Q R, Yu M, He Y D and Wu W G 2018 *IEEE Electron Dev. Lett.* **39** 1888

[7] Liu S, Cai Y, Gu G, Wang J, Zeng C, Shi W, Feng Z, Qin H, Cheng Z, Chen K J and Zhang B 2012 *IEEE Electron Dev. Lett.* **33** 354

[8] He J B, Hua M Y, Zhang Z F and Chen J K 2018 *IEEE T. Electron. Dev.* **65** 3185

[9] Hashizume T, Nishiguchi K, Kaneki S, Kuzmik J and Yatabe Z 2018 *Mater. Sci. Semicond. Proc.* **78** 85

[10] Long R D, Jackson C M, Yang J, Hazeghi A, Hitzman C, Majety S, Arehart A R, Nishi Y, Ma T P, Ringel S A and Mclntyre P C 2013 *Appl. Phys. Lett.* **103** 201607

[11] Liu C, Chor E F and Tan L S 2006 *Appl. Phys. Lett.* **88** 173504

[12] Kanamura M, Ohki T, Kikkawa T, Imanishi K, Imada T, Yamada A and Hara N 2010 *IEEE Electron Dev. Lett.* **31** 189

[13] Huang S, Yang S, Roberts J and Chen K J 2011 *Jpn. J. Appl. Phys.* **50** 110202

[14] Choi W, Seok O, Ryu H, Cha H and Seo K 2014 *IEEE Electron Dev. Lett.* **35** 175

[15] Zhao Y P, Wang C, Zheng X F, Ma X H, He Y L, Liu K, Li A, Peng Y, Zhang C F and Hao Y 2020 *Phys. Status Solidi A* **217** 1900981

[16] Tapajna M and Kuzmik J 2012 *Appl. Phys. Lett.* **100** 113509

[17] Chou B Y, Hsu W C, Liu H Y, Ho C S and Lee C S 2013 *Semicond. Sci. Technol.* **28** 074005

[18] Yoon Y J, Kang H S, Seo J H, Kim Y J, Bae J H, Lee J H, Kang I M and Cho S J 2014 *J. Korean Phys. Soc.* **65** 1579

[19] Zhao Y P, Wang C, Zheng X F, Ma X H, He Y L, Liu K, Li A, Peng Y, Zhang C F and Hao Y 2020 *Solid-State Electron.* **163** 107649

[20] Zhu J J, Ma X H, Xie Y, Hou B Chen W W, Zhang J C and Hao Y 2015 *IEEE T. Electron. Dev.* **62** 512

[21] He Y L, Gao H, Wang C, Zhao Y P, Lu X L, Zhang C F, Zheng X F, Guo L X, Ma X H and Hao Y 2019 *Phys. Status Solidi A* **216** 1900115